Asian Journal of Chemistry; Vol. 38, No. 1 (2026), 114-122
ASIAN JOURNAL OF CHEMISTRY
https://doi.org/10.14233/ajchem.2026.34892

Utilization of Bengal Quince Leaf Biomass in Adsorptive Removal of Toxic Methylene Blue Dye: Influence of System Parameters and Kinetic Study

ARKOJYOTI MAJUMDAR[1], BASANTA K. DAS[2], MEHDI AL KAUSOR[1,3] and SHARMISTHA CHAKRABORTY[1,3,*]

[1]Department of Chemistry, Bodoland University, Kokrajhar-783370, India
[2]Department of Chemistry, Kokrajhar Govt. College, Kokrajhar-783370, India
[3]Department of Chemistry, Science College, Kokrajhar-783370, India

*Corresponding author: E-mail: chakrabortysharmisthakjh@gmail.com

Received: 14 September 2025 *Accepted*: 11 November 2025 *Published online*: 31 December 2025 AJC-22229

Methylene blue (MB) has been identified as harmful to human health, potentially causing various adverse effects, including gastritis, irritation of the eyes, irritation of the skin, leptomeningeal inflammation, neuronal apoptosis, increased heart rate, nausea, vomiting and diarrhoea. Therefore, the treatment of wastewater that contains such dye is crucial due to its detrimental impact. Herein, in a batch setup, Bengal quince leaf powder (BQLP) was assessed for its capacity in removing MB from aqueous medium along with the impacts of some influential factors. The equilibrium data fit well (R^2 = 0.9931) with Langmuir isotherm model, confirming the viability of BQLP as an adsorbent. The maximum monolayer adsorption efficacy (q_{max}) of the bioadsorbent was emerged as 175.44 mg g^{-1} with a Langmuir isotherm constant of 41.83 L mg^{-1}, highlighting the efficiency of BQLP in dye removal. The kinetics study indicated that the observed data aligns with pseudo-first-order kinetics (R^2 = 0.9714) and intraparticle diffusion models (R^2 = 0.9797) with a pseudo-first-order rate constant of 4.2×10^{-2} min^{-1}. The study demonstrates that BQLP as an effective biosorbent in removing MB dye from the aqueous medium. The enhanced is attributed to stronger electrostatic attractions, hydrogen bonding, n–π interactions and π–π stacking. Overall, the findings of this investigation indicate that BQLP is a promising, facile and eco-friendly adsorbent for wastewater treatment, offering an effective means of mitigating the environmental hazards posed by synthetic dyes such as MB. Future study should focus on evaluating the regeneration efficiency, reusability and scalability of BQLP to support its potential deployment in large-scale industrial wastewater management.

Keywords: Bioadsorbent, Adsorption, Bengal quince leaf, Dye, Methylene blue.

INTRODUCTION

Organic dyes are the complex chemical compounds used to impart colour to various materials, binding to textiles or surfaces to produce stable and vibrant hues. Valued for their broad applicability and favourable properties, they play a significant role in global industries, particularly in printing, textiles, food processing, and cosmetics, where their ability to deliver intense and long-lasting colours is essential [1]. Such dyes are also utilized in groundwater tracing, environmental monitoring and pharmaceutical applications. Among other industries, the textile and dye-manufacturing industries are responsible for releasing a significant portion of dyes to the environment [2].

Methylene blue (MB) is a widely used cationic, monovalent thiazine dye characterized by its blue colour, heterocyclic aromatic structure and molecular formula $C_{16}H_{18}N_3SCl$. Owing to its high-water solubility, MB is extensively employed in textile industries for fabric colouration and leather dyeing applications [3]. Although generally considered to have low acute toxicity, exposure to MB can nonetheless result in a range of adverse health effects, including acute haemolysis, gastrointestinal disturbances, convulsions, irritation of the eyes and skin, leptomeningeal inflammation, neuronal apoptosis, cognitive impairment, and cardiovascular symptoms such as tachycardia, along with nausea and vomiting [4,5]. The complex aromatic structures of many organic dyes make them chemically stable and resistant to degradation, thereby complicating their removal from the environment [6]. Wastewater contaminated with such dyes poses significant risks to human health due to their toxicological effects. In particular, ingestion of water containing MB can lead to cyanosis, jaundice,

elevated heart rate, shock, vomiting and other adverse symptoms [7]. Owing to their harmful impact on a wide range of living organisms, dye-laden effluents remain a major environmental and public-health concern. Therefore, the removal of synthetic dyes such as MB from aqueous media is essential, prompting extensive research into suitable treatment methods. Techniques such as biological degradation, reverse osmosis, membrane filtration, ion exchange, coagulation–precipitation and adsorption are commonly employed to eliminate dye pollutants from wastewater [8-11]. Among these, adsorption remains one of the most effective and widely used approaches due to its simplicity, efficiency, and compatibility with a broad range of adsorbent materials.

A wide range of non-traditional, low-cost materials such as clays, plant-derived substances, biosorbents and various industrial or agricultural wastes have been reported as effective sorbents for dye removal [12-14]. Although activated carbons derived from biomass exhibit excellent adsorption capacity, their high production cost limits large-scale application [15]. Consequently, the search for inexpensive and efficient alternatives for MB removal continues, with numerous agricultural byproducts including rice husk, orange and citrus peels, barley husk, sawdust, cereal chaff, castor seed shells, pine cones and pine needles already explored for this purpose [16-21]. In this study, the eco-friendly preparation of a low-cost bioadsorbent derived from Bengal quince (*Aegle marmelos*) leaf powder is reported and evaluated its performance in removing toxic MB dye from wastewater. The material was characterized using standard spectroscopic techniques and the adsorption behaviour was examined through systematic studies on the effects of operational parameters, adsorption isotherms, and kinetic models to assess its overall efficiency.

EXPERIMENTAL

Analytical-grade methylene blue (Sigma-Aldrich, India) was employed without further purification. A stock solution (1 1 g L^{-1}) was prepared in deionized water and working solutions of desired concentrations were obtained by serial dilution. Dye concentrations were determined using a VWR® 6300PC UV-Vis spectrophotometer at λ_{max} = 664 nm. A calibration curve was constructed by plotting absorbance *versus* known MB concentrations and was subsequently used for quantitative analysis of unknown samples.

Mature Bengal quince (*Aegle marmelos*) leaves were collected from Dhubri District (26.0983º N, 90.1151º E), India. The freshly leaves were thoroughly washed with distilled water to remove surface impurities, shade-dried and then oven-dried at 100-110 ºC for 3-5 h until brittle. The dried material was ground to a fine powder and repeatedly washed with distilled water to remove soluble constituents and pigments until the washings became colourless. The residue was oven-dried at 100-110 ºC for 4 h, sieved and particles smaller than 100 µm were collected. The resulting material was designated as Bengal quince leaf powder (BQLP) and used as the bioadsorbent in subsequent adsorption studies.

Characterization: Powder X-ray diffraction (PXRD) spectra of the adsorbent were taken by Empyrean Power X-ray diffractometer (Make: PANalytical, Model: Zetium). Fourier transformation infrared (FTIR) spectra were obtained through BRUKER Optik GmbH, Model: TENSOR 27 instrument. Scanning Electron Microscopic (SEM) images were obtained by SEM instrument (Make: Zeiss Model: Σigma VP). The surface area was obtained by N_2-adsorption/desorption method using BET equation at 77 K with the help of Quantachrome Autosorb-1C Surface-area analyzer.

Batch adsorption study: The batch adsorption studies were achieved by addition of a calculated amount of BQLP material to a specified quantity of the MB dye pollutant in 250 mL conical flasks. The mixture was then agitated at 125 rpm for 150 min using a water bath shaker machine maintained at 298 K. The solutions were taken out at the scheduled time and subsequently centrifuged. A UV-visible spectrophotometer standardization curve has been used to quantify concentration of the remaining MB dye in the solution. The percentage removal of the dye was determined by the following equation:

$$\text{Removal (\%)} = \frac{C_o - C_t}{C_o} \times 100 \quad (1)$$

The amount of dye (q_t, mg g^{-1}) adsorbed onto BQLP at time was calculated using the following equation:

$$q_t = \frac{(C_o - C_t)V}{m} \quad (2)$$

where V is the volume of the solution in L m is the mass of BQLP in g; C_0 is the initial concentration of MB in mg L^{-1}; and C_t is the concentration of dye at time t.

Adsorption isotherm studies: In this study, adsorption isotherm analysis was conducted to evaluate the equilibrium adsorption behaviour and capacity of BQLP. In this study, four isotherm models were applied to interpret the experimental data, enabling systematic assessment of surface characteristics, adsorption mechanism, saturation behaviour and to identify favourable conditions for efficient dye removal

Langmuir isotherm: In this model, adsorption is assumed to proceed *via* monolayer coverage on a finite number of energetically homogeneous sites of the adsorbent surface. The following equation represents the linear form of Langmuir adsorption isotherm:

$$\frac{1}{q_e} = \left(\frac{1}{K_L q_{max}}\right)\frac{1}{C_e} + \frac{1}{q_{max}} \quad (3)$$

where q_e represents the amount of adsorbed dye at equilibrium; C_e represents the equilibrium concentration of MB; q_{max} represents maximum adsorption efficiency; and K_L represents Langmuir isotherm constant [22].

Freundlich isotherm: This isotherm assumes adsorption on a heterogeneous surface characterized by non-uniform active sites and a distribution of adsorption energies. The linear form of Freundlich adsorption isotherm is written as:

$$\ln q_e = \ln K_F + \frac{1}{n}\ln C_e \quad (4)$$

where Q_e represents quantity of the adsorbed (mg L^{-1}) at equilibrium; K_p represents adsorption constant's capacity; C_e represents the concentration of MB at equilibrium and; n represents the intensity constant of adsorption [23].

Temkin isotherm: The model assumes that the heat of adsorption varies linearly with surface coverage of the adsorbate [24]. Specifically, it postulates a linear decline in the heat of adsorption with increasing coverage, neglecting deviations at very low and very high loadings, rather than the logarithmic dependence on coverage proposed in other models [25].

$$q_e = \frac{RT}{b} \ln C_e + \frac{RT}{b} \ln K_T \quad (5)$$

where K_T represents equilibrium binding constant (L mg^{-1}); T represents temperature; b represents the Temkin constant; and RT/b relates to heat of sorption (J mol^{-1}).

Dubinin-Radushkevich (D-R) isotherm The Dubinin–Radushkevich (D–R) isotherm, based on Polanyi's potential theory, assumes a Gaussian distribution of adsorption energies within the microporous structure of the adsorbent [26]. The isotherm is given by:

$$\ln q_e = \ln q_{max} - K_{DR}\varepsilon^2 \quad (6)$$

where q_e represents the quantity of dye adsorbed at equilibrium; C_e represents the concentration of MB at equilibrium; q_{max} represents the maximum adsorption efficiency. And the Polanyi adsorption potential (ε) is defined as:

$$\varepsilon = RT \ln 1 + \frac{1}{C_e} \quad (7)$$

where K_{DR} is a constant related to adsorption energy; R is the molar gas constant; and T is the temperature.

Kinetics study: The adsorption kinetics were investigated using the pseudo-first-order (PFO) and pseudo-second-order (PSO) models to describe the adsorption rate. In addition, the experimental data were analyzed using the intraparticle diffusion (IPD) model to identify the rate-determining step. Eqns. 8 and 9 represent the PSO and PFO kinetic models, respectively, used to evaluate the experimental adsorption rate.

$$\ln(q_e - q_t) = \ln q_e - k_1 t \quad (8)$$

$$\frac{t}{q_t} = \frac{1}{k_2} \frac{1}{q_e^2} + \frac{t}{q_e} \quad (9)$$

where q_e represents the quantity of dye (mg g^{-1}) adsorbed in equilibrium, q_t represents the same at time t, while k_1 and k_2 represents the rate constant of adsorption (PFO and PSO) in min^{-1}.

The IPD model was also used to verify the rate by fitting the data in the expression shown in eqn. 10.

$$q_t = k_i \sqrt{t} + C_i \quad (10)$$

where k_i denotes the intraparticle diffusion (IPD) rate constant (mg g^{-1} min^{-1}), determined from the slope of the plot of q_t *versus* C_i. The intercept of this plot reflects the influence of the boundary layer at the interface between the adsorbent surface (BQLP) and the dye molecules.

RESULTS AND DISCUSSION

XRD studies: This PXRD study explores the changes in structural characteristics of the materials before and after adsorption (Fig. 1). The particle size and lattice strain were calculated using the Scherrer's equation and the Williamson-Hall plot method [27]. Lattice constants, which define the unit cell dimensions, are crucial for understanding the structural framework and intermolecular interactions of materials, particularly in adsorption studies where even minor variations can markedly influence performance. In present study, the material exhibited a hexagonal lattice structure in both cases, with lattice constants of a = 6.709 Å before adsorption and a = 6.709 Å after adsorption. However, significant differences in the crystallite size were observed. After adsorption, the material exhibited a larger crystallite size (38.91 nm) and lower lattice strain (0.350), indicating improved crystalline quality. In contrast, before adsorption, it showed a smaller crystallite size (24.42 nm) and higher lattice strain (0.556), reflecting increased lattice distortions or defect density.

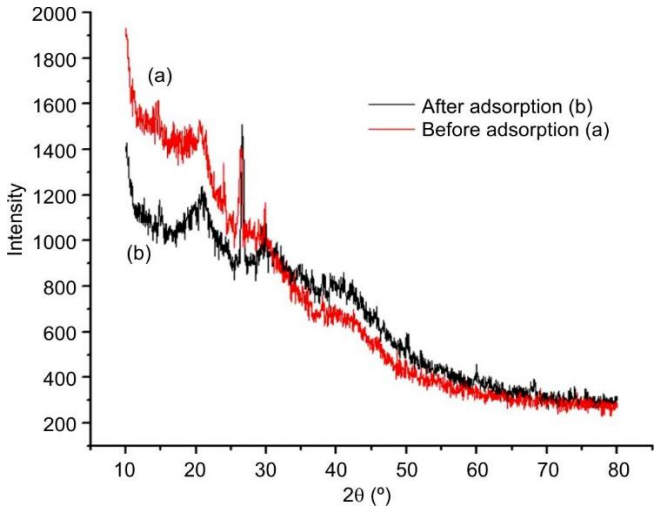

Fig. 1. XRD patterns of Bengal quince leaf biomass before (a) and after (b) adsorption

These results are consistent with previous studies showed that smaller crystallite sizes are associated with higher lattice strain due to increased defect density and surface-to-volume ratio, as observed in alumina–zirconia nanocomposites where XRD peak broadening reflects both size reduction and lattice distortion [28]. The higher defect density before adsorption likely enhances adsorption activity, whereas the reduced strain and improved crystallinity after adsorption favour structural stability. Lattice strain is known to influence electronic properties and adsorption energies, thereby affecting adsorption performance [29]. The slight variation in lattice constants further highlights the role of structural relaxation and strain in governing adsorbate–host interactions, consistent with earlier reports emphasizing the importance of structural parameters in adsorption applications [30,31].

FTIR studies: Fig. 2 display the FTIR spectra of the adsorbent before and after adsorption. In the after-adsorption spectrum, pronounced band broadening and increased absorption in the O–H/N–H stretching region (≈3500-3200 cm^{-1}) indicate strong hydrogen-bonding interactions between the adsorbate and surface hydroxyl groups, consistent with previous reports [32]. Enhanced or newly appearing peaks in the 1600-1500 cm^{-1} region suggest the presence of aromatic or amide

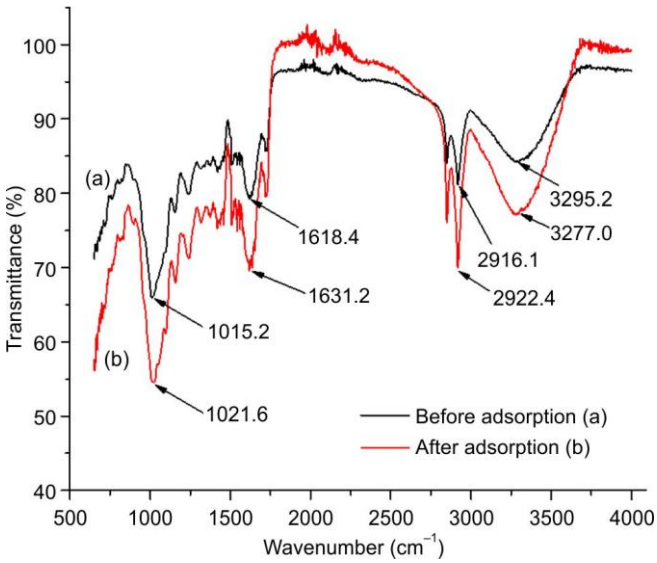

Fig. 2. FTIR spectra of Bengal quince leaf biomass before (a) and after (b) adsorption

functionalities, attributable to adsorbed organic species or nitrogen-containing groups [33]. The bands at 2916 and 3291 cm^{-1} correspond to symmetric and asymmetric aliphatic C–H stretching vibrations [34]. A moderate peak near 1612 cm^{-1} is assigned to C=O stretching of carboxyl groups involved in intermolecular hydrogen bonding, reflecting the coexistence of ionized and non-ionized –COO^{-} species [35]. A strong band at 1022-1014 cm^{-1} is attributed to C–O–C stretching vibrations [36].

Moreover, increased absorption in the fingerprint region (1300-1000 cm^{-1}) indicates the formation or enhancement of C–O and/or C–N vibrational modes, supporting the occurrence of multiple interaction mechanisms such as hydrogen bonding, electrostatic attraction and possible π–π interactions. The overall decrease in transmittance confirms effective surface coverage, consistent with the observed adsorption performance and earlier adsorption studies on functionalized materials [37].

SEM: The SEM images in Fig. 3 reveal that fresh BQLP possesses a rough, uneven surface with few visible pores but numerous surface irregularities, providing multiple sites for MB adsorption. In contrast, the micrographs of MB-loaded BQLP show visible changes in surface morphology, reflecting the attachment of dye molecules. SEM, often combined with energy-dispersive X-ray (EDX) analysis, is a valuable tool for elucidating adsorbent structure and understanding interactions with adsorbates such as MB.

EDX analysis further provides elemental insights into both fresh and MB-loaded biosorbents. As shown in Fig. 4, the fresh BQLP contains primarily carbon and oxygen, while the MB-loaded sample exhibits additional nitrogen, calcium, and silicon signals. These observations confirm the binding of MB to the biosorbent surface and highlight the structural and compositional modifications that occur during adsorption, offering a deeper understanding of the biosorption mechanism.

BET surface area analysis: The N_2 adsorption isotherm before adsorption process was characterized by a stable rise in adsorption volume with relative pressure, peaking at 11.79 cc/g at $P/P_0 \approx 0.988$, which is an indicative of mesoporous materials with high adsorption capacity (Fig. 5a). This behaviour aligns with Type-IV isotherms, typical of mesoporous structures, as classified by IUPAC [38]. In contrast, after adsorption (Fig. 5a) lower adsorption volumes, with a maximum of 8.64 cc/g at the same relative pressure, reflect reduced pore availability due to adsorbate retention. This observation aligns with previous studies showing that adsorbate molecules can block pores, reducing adsorption capacity in post-adsorption isotherms [38]. The BET C-constant increased from 4.225 before adsorption to 6.011 after adsorption, indicating stronger adsorbate–adsorbent interactions. Higher C values reflect increased affinity between the adsorbate and adsorbent, consistent with thermodynamic studies of adsorption processes. Together, the observed changes in surface area, adsorption capacity and interaction strength confirm the material's efficiency in capturing adsorbates and underscore its potential for adsorption-based applications.

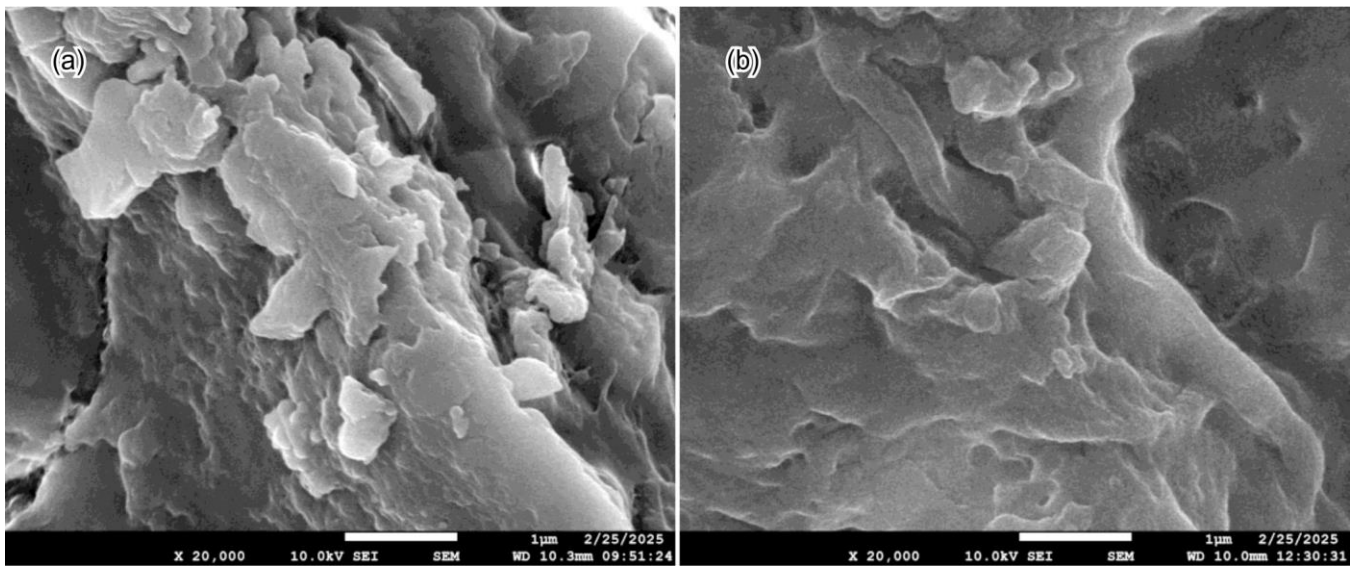

Fig. 3. SEM images of (a) distilled water washed BQLP and (b) methylene blue treated BQLP

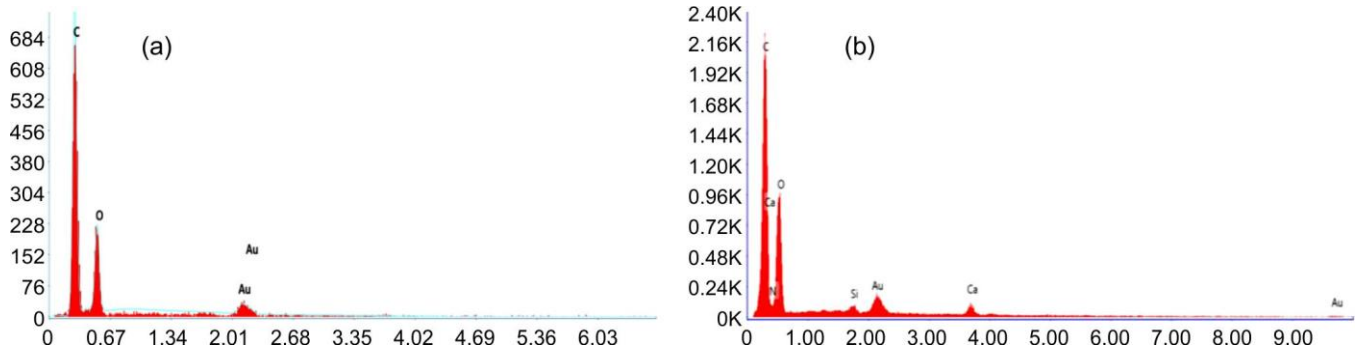

Fig. 4. EDX spectra of elemental composition (a) before adsorption and (b) after adsorption

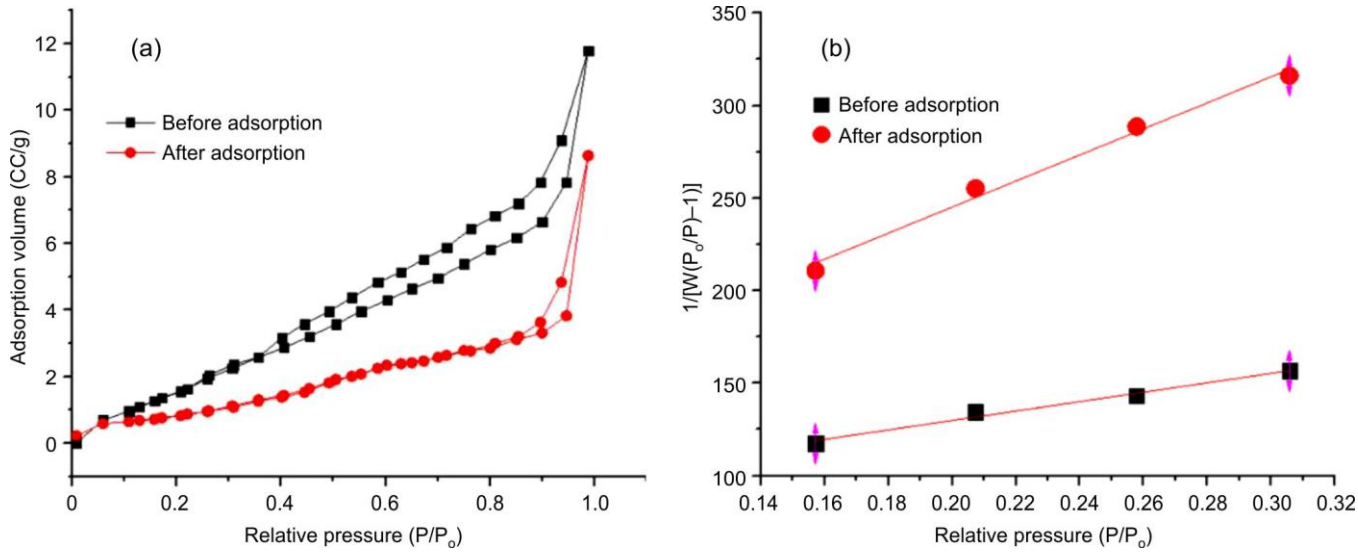

Fig. 5. (a) BET isotherm of BQLP and (b) plot of $\frac{1}{2a[W((P_o/P)-1]}$ against relative pressure

The specific surface area was found from the plot of $\frac{1}{2a[W((P_o/P)-1)]}$ against relative pressure is shown in Fig. 5b. It was observed that the observed decrease in specific surface area from 10.442 m^2/g to 4.628 m^2/g after adsorption, which indicates significant pore occupation by the adsorbate. This reduction is consistent with findings in adsorption studies where pore filling leads to decreased surface areas post-adsorption. For instance, research on activated carbons has shown similar trends, where adsorbate molecules occupy the pores, resulting in reduced surface areas [39].

Adsorption studies: It is well established that the system parameters such as contact time, initial dye concentration, adsorbent dose and solution pH significantly influence adsorption. In this study, the effects of these parameters on MB removal using BQLP were investigated to determine optimal conditions.

Effect of contact time: As shown in Fig. 6a, MB removal occurs rapidly at the initial stages due to the availability of abundant active sites, and gradually slows until equilibrium is reached at approximately 150 min.

Effect of initial dye concentration: Fig. 6b shows that increasing the initial MB concentration from 60 to 100 mg L^{-1} decreases the percentage removal from 95.3% to 70.6% at equilibrium. At higher concentrations, the ratio of dye molecules to available adsorption sites increases, limiting the capacity of adsorbent and reducing overall removal efficiency [40].

Effect of adsorbent dose: The influence of adsorbent dosage is shown in Fig. 6c. Increasing BQLP dose from 0.5 to 1.5 g L^{-1} enhances the removal of MB from 79.9% to 95.3% due to more available surface-active sites. However, further increasing the dose to 2.0 g L^{-1} slightly reduces removal to 92.4%, likely due to particle agglomeration hindering access to active sites [41].

Effect of pH: Fig. 6d illustrates that the removal of MB is higher in acidic medium (95.3%) than in basic medium (77.7%). This is attributed to the protonation of MB molecules at lower pH, which enhances electrostatic attraction to the adsorbent surf-ace, whereas deprotonation at higher pH reduces adsorption [42].

These results collectively highlight the importance of optimizing system parameters to maximize adsorption efficiency.

Adsorption isotherms study: Adsorption isotherms describe the equilibrium distribution of molecules between liquid and solid phases. To study the isotherms, 100 mL of MB solution with varying concentrations (20-100 mg L^{-1}) was treated with 0.15 g of BQLP at constant shaking and

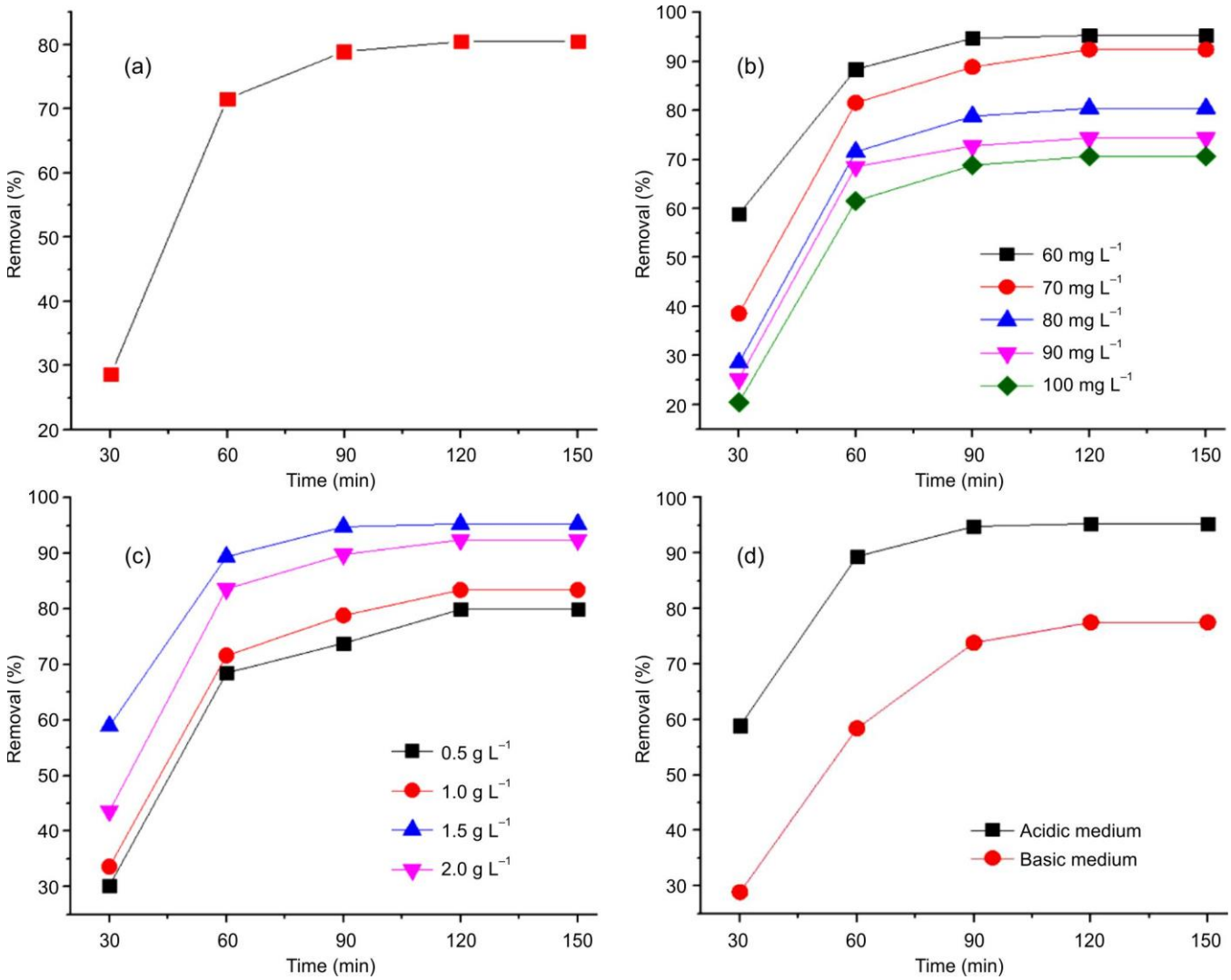

Fig. 6. Effects of (a) contact time [C_o = 60 mg L^{-1}, w = 1.5 g, shaking speed 125 rpm, T = 30 ºC, pH = 3.5], (b) initial concentration [w = 1.5 g L^{-1}, shaking speed 125 rpm, T = 30 ºC, pH = 3.5], (c) adsorbent dose [C_o = 60 mg L^{-1}, T = 30 ºC, shaking speed 125 rpm, pH = 3.5], (d) pH [C_o = 60 mg L^{-1}, T = 30 ºC, shaking speed 125 rpm] on adsorption of MB removal onto BQLP adsorbent

temperature for 150 min, exceeding equilibrium time, while other conditions were kept constant. Equilibrium adsorption capacity (q_e) and related parameters were calculated using the specified equations and the data were fitted to various isotherm models.

Langmuir isotherm: The linearized Langmuir plot of $1/q_e$ *versus* $1/C_e$ (Fig. 7a) yielded a maximum adsorption capacity (q_{max}) of 175.44 mg g^{-1} and a Langmuir constant (K_L) of 41.83 L mg^{-1}, indicating strong binding affinity. The high correlation coefficient (R^2 = 0.9931) confirms monolayer adsorption on a homogeneous surface with finite sites, demonstrating effectiveness of BQLP in MB removal.

Freundlich isotherm: The linearized plot of ln q_e *versus* ln C_e (Fig. 7b) gave a Freundlich constant (K_F) of 16.92 mg g^{-1} and intensity factor n = 2.8, indicating moderate adsorption capacity under less favourable conditions. The correlation coefficient (R^2 = 0.7966) suggests a poor fit, reflecting surface heterogeneity.

Temkin isotherm: The Temkin model (Fig. 7c) assumes adsorption heat decreases with surface coverage due to the adsorbate–adsorbate interactions. The adsorption heat constant (b = 304.19 J mol^{-1}) and equilibrium binding constant (K_T = 10.23 L g^{-1}) indicate moderate interactions. With R^2 = 0.8609, the model suggests heterogeneous adsorption with progressively decreasing binding energies, offering insight into the interaction forces.

Dubinin-Radushkevich (D-R) isotherm: The D-R analysis (Fig. 7d) distinguishes between physical and chemical adsorption. The maximum adsorption capacity (q_{max} = 39.50 mg g^{-1}) and the D-R constant (K_{DR} = 484.24 mol^2 J^{-2}) suggest a physisorption mechanism. The linear regression of ln qe versus ε^2 shows good correlation, though R^2 = 0.8363 indicates a weaker fit.

Overall, Langmuir fitting indicates predominant monolayer adsorption, while Temkin and D-R models provide insights into heterogeneous surface interactions and adsorption energetics. A comparison with similar MB adsorption studies is summarized in Table-1.

Adsorption kinetics studies: The kinetics of adsorption was investigated by fitting the investigational data in PFO

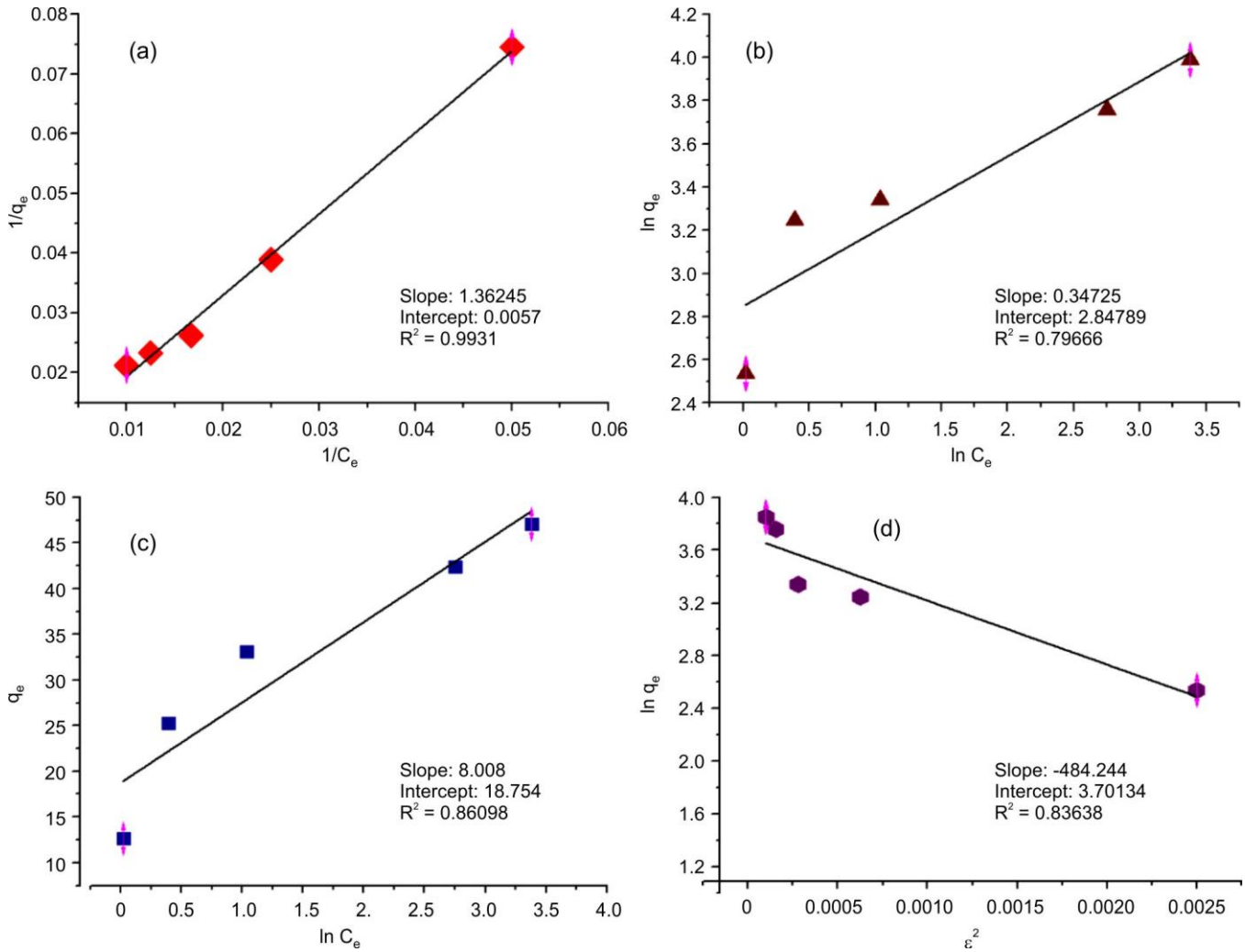

Fig. 7. Plots of isotherm models: (a) Langmuir, (b) Freundlich, (c) Temkin, and (d) Dubinin-Radushkevich for adsorption of MB removal onto BQLP [conditions: concentraction = 20-100 mg L^{-1}, weight = 1.5 g, shaking speed = 125 rpm, T = 30 ºC]

TABLE-1
COMPARISON DATA OF q_{max} VALUES OF SOME PLANT LEAF-BASED ADSORBENTS USED IN REMOVAL OF MB DYE BY ADSORPTION

Adsorbent (source)	Initial dye concentration (mg L^{-1})	Adsorbent dose (g L^{-1})	Equilibrium time (min)	Temp. (K)	q_{max} (mg g^{-1})	Ref.
Pine leaves (*Pinus roxburghii*)	60	0.04	180	300	36.88	[43]
Neem leaves (*Azadirachta indica*)	50	2.00	180	300	60.60	[44]
Tea leaves (*Camellia sinensis*)	30	0.04	20 h	–	68.28	[45]
Ashoka leaves (*Saraca asoca*)	50	2.50	50	303	90.9	[46]
Kadamba leaves (*Neolamarckia cadamba*)	50	4.00	50	303	101.4	[47]
Banana leaves (*Musa sapientum*)	250	1.50	280	303	109.89	[48]
Litchi leaves (*Litchi chinensis*)	50	1.00	60	300	119.76	[49]
Bengal quince leaves (*Aegle marmelos*)	60	1.50	150	303	175.44	Present study

and PSO kinetic models to explain adsorption rate and the data were subjected to the IPD model (Fig. 8c) to verify the rate determining step. The relevant information obtained from the kinetic study (Fig. 8a-b) are presented in Table-2 Furthermore, the separation factor (R_L) values for different dye concentrations were inside the favourable range ($0 < R_L < 1$), indicating the spontaneous and favourable adsorption process. The R^2 value specifies that the investigational data was highly interrelated with PFO model but did not correlate well with PSO model. The first-order kinetics constant *i.e.* k_1 is found to be 4.2×10^{-2} min^{-1} and q_e is calculated as 50.47 mg g^{-1} from the plot respectively. Since the value of R^2 = 0.97971 is very close to 1, so the IPD model seems to be fit well for the experiment. The rate constant of IPD model, k_i is calculated as 5.0040 mg g^{-1} min^{-1}. The results revealed that there is a strong influence of the boundary layer on the interface between the BQLP surface and the dye particles.

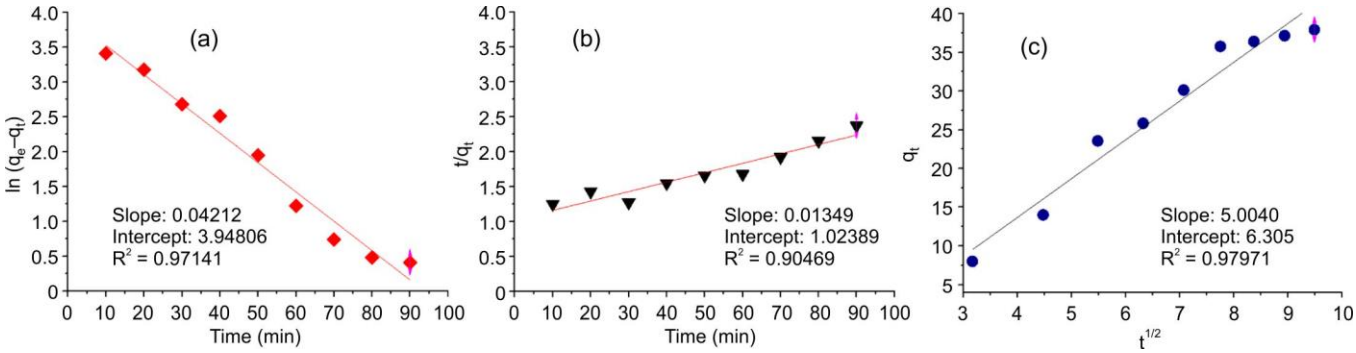

Fig. 8. Kinetic plots of the adsorption process (a) pseudo-first-order, (b) pseudo-second-order, (c) inter particle diffusion model

TABLE-2
Values OF PARAMETERS ASSOCIATED WITH THE KINETIC MODELS APPLIED IN THIS STUDY

Pseudo-first-order		Pseudo-second-order		Inter particle diffusion	
k_1 (min^{-1})	4.2×10^{-2}	k_2 (mg^{-1} g min^{-1})	1.7×10^{-4}	k_i (mg^{-1} g min^{-1})	5.0040
q_e (mg g^{-1})	50.47	q_e (mg g^{-1})	74.1	Ci (mg g^{-1})	6.305
R^2	0.97141	R^2	0.90469	R^2	0.97971

Mechanism: The possible interactions involved between BQLP and MB dye molecules are primarily mediated by the existence of diverse functional groups such as hydroxyl (-OH), carboxyl (-COOH) and carbonyl (>C=O), which act as active sites on the adsorbents surface. The process is primarily driven by electrostatic attraction between the negatively charged BQLP surface and the cationic MB dye. Moreover, hydrogen bonding occurs between the lone pair of electrons on the nitrogen atom of MB and the functional groups on BQLP. The adsorption is further stabilized through n–π interactions, where lone pairs on oxygen atoms of BQLP delocalize into the π-orbitals of MB's aromatic rings, and through π–π stacking between the aromatic rings of BQLP and MB, resulting in a synergistic mechanism that enhances the overall uptake of the dye [49,50]. Based on these facts, the probable mechanism of adsorption of MB on to BQLP is shown in Fig. 9.

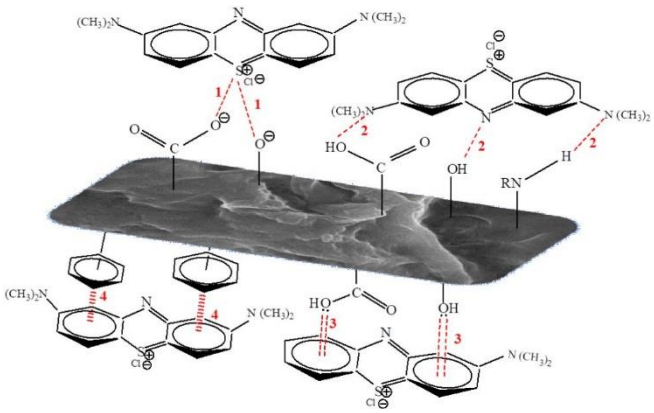

Fig. 9. Mechanism of adsorption of MB dye on to BQLP; [**1**: electrostatic interactions; **2**: hydrogen bonding; **3**: n–π interactions; **4**: π–π stacking]

Conclusion

The study demonstrates that Bengal quince leaf (BQLP) is an efficient biosorbent for the methylene blue (MB) dye removal from aqueous solutions. The investigational data fits well with Langmuir isotherm model, confirming viability of the BQLP as an adsorbent. The maximum monolayer adsorption efficiency was obtained as 175.44 mg g^{-1}, highlighting the efficiency of BQLP in dye removal. The kinetics study revealed that the investigational data fits well in pseudo-first-order kinetics and intraparticle diffusion models. The separation factor (R_L) values for different dye concentrations were within the favourable range ($0 < R_L < 1$), indicating the impulsive and favourable adsorption process. The findings of the study suggest that BQLP can be a cost-effective and eco-friendly alternative for wastewater treatment, reducing the environmental hazards associated with synthetic dyes like MB. Future studies can explore the regeneration potential and scalability of BQLP for large-scale applications in industrial wastewater management.

ACKNOWLEDGEMENTS

The authors gratefully acknowledge SAIF, Gauhati University, SAIC, Tezpur University and Material Analysis & Research Centre, Bengaluru for characterization.

CONFLICT OF INTEREST

The authors declare that there is no conflict of interests regarding the publication of this article.

DECLARATION OF AI-ASSISTED TECHNOLOGIES

During the preparation of this manuscript, the authors used an AI-assisted tool(s) to improve the language. The authors reviewed and edited the content and take full responsibility for the published work.

REFERENCES

1. H.B. Slama, A. Chenari Bouket, Z. Pourhassan, F.N. Alenezi, A. Silini, H. Cherif-Silini, T. Oszako, L. Luptakova, P. Golińska and L. Belbahri, *Appl. Sci.*, **11**, 6255 (2021); https://doi.org/10.3390/app11146255

2. M.M. Islam, A.R. Aidid, J.N. Mohshin, H. Mondal, S. Ganguli and A.K. Chakraborty, *Cleaner Chem. Eng.*, **11**, 100165 (2025); https://doi.org/10.1016/j.clce.2025.100165
3. I. Khan, K. Saeed, I. Zekker, B. Zhang, A.H. Hendi, A. Ahmad, S. Ahmad, N. Zada, H. Ahmad, L.A. Shah, T. Shah and I. Khan, *Water*, **14**, 242 (2022); https://doi.org/10.3390/w14020242
4. T.K. Sen, S. Afroze and H.M. Ang, *Water Air Soil Pollut.*, **218**, 499 (2011); https://doi.org/10.1007/s11270-010-0663-y
5. W.T. Tsai, K.J. Hsien and H.C. Hsu, *J. Hazard. Mater.*, **166**, 635 (2009); https://doi.org/10.1016/j.jhazmat.2008.11.071
6. S. Arabi and M.R. Sohrabi, *Water Sci. Technol.*, **70**, 24 (2014); https://doi.org/10.2166/wst.2014.189
7. A.K. Kushwaha, N. Gupta and M.C. Chattopadhyaya, *J. Saudi Chem. Soc.*, **18**, 200 (2014); https://doi.org/10.1016/j.jscs.2011.06.011
8. Ç. Sarıcı Özdemir, *Sep. Sci. Technol.*, **54**, 3046 (2019); https://doi.org/10.1080/01496395.2019.1565769
9. M.M. Hassan and C.M. Carr, *Chemosphere*, **209**, 201 (2018); https://doi.org/10.1016/j.chemosphere.2018.06.043
10. Q. Wei, Y. Zhang, K. Zhang, J.I. Mwasiagi, X. Zhao, C.W. Chow and R. Tang, *Korean J. Chem. Eng.*, **39**, 1850 (2022); https://doi.org/10.1007/s11814-021-1056-1
11. K. Jankowska, Z. Su, J. Zdarta, T. Jesionowski and M. Pinelo, *J. Hazard. Mater.*, **435**, 129071 (2022); https://doi.org/10.1016/j.jhazmat.2022.129071
12. O.S. Bello, K.A. Adegoke, A.A. Olaniyan and H. Abdulazeez, *Desal. Water Treat.*, **53**, 1292 (2015); https://doi.org/10.1080/19443994.2013.862028
13. S.T. Al-Asadi, F.F. Al-Qaim, H.F. Al-Saedi, I.F. Deyab, H. Kamyab and S. Chelliapan, *Environ. Monit. Assess.*, **195**, 676 (2023); https://doi.org/10.1007/s10661-023-11334-2
14. B.N. Shelke, M.K. Jopale and A.H. Kategaonkar, *J. Indian Chem. Soc.*, **99**, 100530 (2022); https://doi.org/10.1016/j.jics.2022.100530
15. S. Radoor, J. Karayil, A. Jayakumar, J. Parameswaranpillai, J. Lee and S. Siengchin, *Sci. Rep.*, **12**, 20580 (2022); https://doi.org/10.1038/s41598-022-22936-0
16. M. Raninga, A. Mudgal, V.K. Patel, J. Patel and M.K. Sinha, *Mater. Today Proc.*, **77**, 286 (2023); https://doi.org/10.1016/j.matpr.2022.11.358
17. Q. Ghzal, T. Javed and M. Batool, *Environ. Sci. Water Res. Technol.*, **9**, 2925 (2023); https://doi.org/10.1039/D3EW00392B
18. A.G. Gurer, K. Aktas, M.O. Akcetin, A.E. Unsar and M. Asilturk, *Water Air Soil Pollut.*, **232**, 138 (2021); https://doi.org/10.1007/s11270-021-05090-7
19. D. Mekuria, A. Diro, F. Melak and T.G. Asere, *J. Chem.*, **2022**, 4849758 (2022); https://doi.org/10.1155/2022/4849758
20. T.M. Eldeeb, U.O. Aigbe, K.E. Ukhurebor, R.B. Onyancha, M.A. El-Nemr, M.A. Hassaan, S. Ragab, O.A. Osibote and A. El Nemr, *Biomass Convers. Biorefin.*, **14**, 9361 (2024); https://doi.org/10.1007/s13399-022-03015-w
21. L.M. Ferreira, R.R. de Melo, A.S. Pimenta, T.K. de Azevedo and C.B. de Souza, *Biomass Convers. Biorefin.*, **12**, 1181 (2022); https://doi.org/10.1007/s13399-020-00660-x
22. M. García-Rollán, E. Sanz-Santos, C. Belver and J. Bedia, *J. Environ. Manage.*, **383**, 125394 (2025); https://doi.org/10.1016/j.jenvman.2025.125394
23. J. Kaushik, V. Kumar, A.K. Garg, P. Dubey, K.M. Tripathi and S.K. Sonkar, *New J. Chem.*, **45**, 9073 (2021); https://doi.org/10.1039/D1NJ00470K
24. M.I. Temkin, *Acta Physicochim. URSS*, **12**, 327 (1940).
25. U.A. Edet and A.O. Ifelebuegu, *Processes*, **8**, 665 (2020); https://doi.org/10.3390/pr8060665
26. M.M. Dubinin, *Dokl. Akad. Nauk SSSR*, **55**, 327 (1947).
27. A.R. West, Solid State Chemistry and its Applications, John Wiley & Sons, edn. 2 (2022).
28. A.K. Deb and P. Chatterjee, *J. Theor. Appl. Phys.*, **13**, 221 (2019); https://doi.org/10.1007/s40094-019-0338-z
29. E. Westsson, S. Picken and G. Koper, *Chem. Commun.*, **55**, 1338 (2019); https://doi.org/10.1039/C8CC09063G
30. M.U. Farooq, M.I. Jalees, A. Iqbal, N. Zahra and A. Kiran, *Desalination Water Treat.*, **160**, 333 (2019); https://doi.org/10.5004/dwt.2019.24173
31. A.E. Kuyucu, A. Selçuk, Y. Önal, İ. Alacabey and K. Erol, *Sci. Rep.*, **15**, 28835 (2025); https://doi.org/10.1038/s41598-025-13685-x
32. Z. Kuodis, I. Matulaitienė, M. Špandyreva, L. Labanauskas, S. Stončius, O. Eicher-Lorka, R. Sadzevičienė and G. Niaura, *Molecules*, **25**, 5633 (2020); https://doi.org/10.3390/molecules25235633
33. N.S. Myshakina, Z. Ahmed and S.A. Asher, *J. Phys. Chem. B*, **112**, 11873 (2008); https://doi.org/10.1021/jp8057355
34. Y.S. Yun, D. Park, J.M. Park and B. Volesky, *Environ. Sci. Technol.*, **35**, 4353 (2001); https://doi.org/10.1021/es010866k
35. R.E. Sievers and J.C. Bailar Jr., *Inorg. Chem.*, **1**, 174 (1962); https://doi.org/10.1021/ic50001a035
36. M. Kumar, G. Elangovan, R. Tamilarasan, G. Vijayakumar, P.C. Mukeshkumar and S. Sendhilnathan, *Pol. J. Chem. Technol.*, **17**, 5 (2015); https://doi.org/10.1515/pjct-2015-0052
37. N. Li, Y. Liu, C. Du, Y. Wang, L. Wang and X. Li, *Sci. Total Environ.*, **861**, 160623 (2023); https://doi.org/10.1016/j.scitotenv.2022.160623
38. O.P. Murphy, M. Vashishtha, P. Palanisamy and K.V. Kumar, *ACS Omega*, **8**, 17407 (2023); https://doi.org/10.1021/acsomega.2c08155
39. F. Ambroz, T.J. Macdonald, V. Martis and I.P. Parkin, *Small Methods*, **2**, 1800173 (2018); https://doi.org/10.1002/smtd.201800173
40. G.K. Sarma, S. Sen Gupta and K.G. Bhattacharyya, *Sep. Sci. Technol.*, **46**, 1602 (2011); https://doi.org/10.1080/01496395.2011.565012
41. W. Tu, Y. Zhou and Z. Zou, *Adv. Funct. Mater.*, **23**, 4996 (2013); https://doi.org/10.1002/adfm.201203547
42. R. Malik, D.S. Ramteke and S.R. Wate, *Waste Manag.*, **27**, 1129 (2007); https://doi.org/10.1016/j.wasman.2006.06.009
43. T.K. Sen, *Processes*, **11**, 1877 (2023); https://doi.org/10.3390/pr11071877
44. S.A. Odoemelam, U.N. Emeh and N.O. Eddy, *J. Taibah Univ. Sci.*, **12**, 255 (2018); https://doi.org/10.1080/16583655.2018.1465725
45. M. El-Azazy, A.S. El-Shafie and B. Al-Shaikh Yousef, *Molecules*, **26**, 6138 (2021); https://doi.org/10.3390/molecules26206138
46. N. Gupta, A.K. Kushwaha and M.C. Chattopadhyaya, *J. Taiwan Inst. Chem. Eng.*, **43**, 604 (2012); https://doi.org/10.1016/j.jtice.2012.01.008
47. S.H. Siddiqui, M.K. Uddin, R. Isaac and O.F. Aldosari, *Adv. Sci. Technol.*, **2022**, 4143138 (2022); https://doi.org/10.1155/2022/4143138
48. R.R. Krishni, K.Y. Foo and B.H. Hameed, *Desalination Water Treat.*, **52**, 6104 (2014); https://doi.org/10.1080/19443994.2013.815687
49. K. Yadav, S.R. Latelwar, D. Datta and B. Jana, *J. Indian Chem. Soc.*, **100**, 100974 (2023); https://doi.org/10.1016/j.jics.2023.100974
50. S. Gul, A. Gul, H. Gul, R. Khattak, M. Ismail, S.U. Khan, M.S. Khan, H.A. Aouissi and A. Krauklis, *Materials*, **16**, 521 (2023); https://doi.org/10.3390/ma16020521